Monitoring Mass Variations in Iraq Using Time-Variable Gravity Data

Othman, Abdullah; Abdelrady, Ahmed ; Mohamed, Ahmed

DOI
10.3390/rs14143346

Publication date
2022

Document Version
Final published version

Published in
Remote Sensing

remote sensing

MDPI

Article

Monitoring Mass Variations in Iraq Using Time-Variable Gravity Data

Abdullah Othman [1], Ahmed Abdelrady [2,*] and Ahmed Mohamed [3]

[1] Department of Environmental Engineering, Umm Al-Qura University, Makkah 21955, Saudi Arabia; agothman@uqu.edu.sa
[2] Faculty of Civil Engineering and Geoscience, Delft University of Technology, 2628 CN Delft, The Netherlands
[3] Department of Geology, Faculty of Science, Assiut University, Assiut 71516, Egypt; ahmedmohamed@aun.edu.eg
* Correspondence: a.r.a.mahmoud@tudelft.nl

Abstract: Iraq is facing a water shortage due to water scarcity and anthropogenic activities. The recent advance in technologies in geophysical methods has made groundwater monitoring possible. Time-variable gravity data and outputs of the climatic model, as well as rainfall data, are integrated to investigate the spatio-temporal mass variations caused by groundwater changes over Iraq. The findings are: (1) For the entire study period (04/2002–12/2020), Period I (04/2002–12/2006), Period II (01/2007–12/2017), and Period III (01/2018–12/2020), the study region had an average annual precipitation rate of 223.4, 252.5, 194.2, and 311.6 mm/y, respectively. (2) The average Terrestrial Water Storage variations (ΔTWSs) varied from -5.79 ± 0.70 to -5.11 ± 0.70 mm/y based on the three different gravity solutions with a mean of -5.51 ± 0.68 mm/y for the entire investigated period. (3) For Periods I, II, and III, the average ΔTWS fluctuation was calculated to be $+6.82 \pm 1.92$, -6.20 ± 1.17, and $+28.58 \pm 12.78$ mm/y, respectively. (4) During the entire period, Periods I, II, and II, the groundwater fluctuation was averaged at -4.86 ± 0.68, $+2.47 \pm 2.20$, -3.79 ± 1.20, and -4.63 ± 12.99 mm/y, respectively, after subtracting the non-groundwater components. (5) At the beginning of the 2007 drought during Period II, a decline in rainfall rate, and significant groundwater withdrawal during Period III all appear to have contributed to groundwater depletion. The Euphrates and Tigris Rivers, as well as the Mesopotamian plain, receive water from the running streams created by the ground relief. The area of the Mesopotamian plain, which has a thicker sedimentary sequence that can reach 9000 m, is found to have a positive TWS signal, indicating that its groundwater potential is higher. The integrated approach is informative and cost-effective.

Keywords: Iraq; time-variable gravity; mass variations; precipitation groundwater

Citation: Othman, A.; Abdelrady, A.; Mohamed, A. Monitoring Mass Variations in Iraq Using Time-Variable Gravity Data. *Remote Sens.* **2022**, *14*, 3346. https://doi.org/10.3390/rs14143346

Academic Editors: Jolanta Nastula and Monika Birylo

Received: 27 May 2022
Accepted: 5 July 2022
Published: 12 July 2022

1. Introduction

Due to its importance for humans and ecosystems, water sustainability is a global issue [1,2]. Anthropogenic water consumption and climatic variables have an impact on water sustainability [3,4]. Around the world, irrigation accounts for 90% of water usage and 70% of water extraction. Arid regions experience significant groundwater depletion [5,6].

The water infrastructure will be under strain by 2050, when the world's population is increased by 22 to 34%, 9.4 to 10.2 billion people. The impact will be made worse by uneven population growth across the country that is unrelated to regional resources. The majority of this population growth will take place in developing nations, initially in Africa and then Asia, where a lack of potable water is already a serious problem [7]. At the moment, just less than half of the world's population, 3.6 billion people (47%) live in locations where water scarcity occurs at least 1 month a year [8]. Moreover, more than half of the world's population (57%) will live in locations where water scarcity occurs at least 1 month a year by 2050. This prediction for water demand, water resources, and water quality is based on some geopolitical issues that are hard to anticipate.

Freshwater resources are currently threatened by scarcity and limitation in several areas, notably in dry and semiarid areas where water scarcity is a problem for both home and agricultural uses [9,10]. Water scarcity is a global issue that has been identified as one of the world's greatest threats by the World Economic Forum [11].

Owing to the increasing heat and aridity, the Middle East is one of the most affected regions of the world in terms of climate change. These conditions are affecting water availability and causing water scarcity. Water scarcity is well-recognized in the Middle East [12,13] and has been a challenging problem since the onset of the 2007 drought [14–16]. In addition to the prevailed dry climatic conditions, the heavy anthropogenic groundwater withdrawal in these regions is a serious problem. Based on a recent [17] report, about 85% of all water is used in the region for irrigation. The lack of water has had a negative impact on almost every Middle Eastern country. Freshwater availability has fallen by 75% since 1950 and is anticipated to decrease by another 50% by 2030 [18]. This is especially true in the case of the three countries (Iran, Iraq, and Saudi Arabia) that were studied by [19].

Physical, chemical, and modelling techniques have all been used to evaluate the rates of recharge and depletion of large hydrogeological settings, including aquifer systems [20–23]. However, these methods are difficult to use on a regional scale due to the scarcity of datasets required for implementation, as well as the time and money required to obtain them, and their findings are occasionally questionable.

The start of the satellite Gravity Recovery and Climate Experiment (GRACE) mission is now measuring the mass variation caused by changes in terrestrial water storage (ΔTWS). The National Aeronautics and Space Administration (NASA) and the German Aerospace Center (GFZ) jointly launched the GRACE project in March 2002. The GRACE mission was launched to take accurate measurements of the Earth's gravity field in order to determine the spatial and temporal fluctuations in the Earth's mass [24] from space. GRACE-derived ΔTWS is a combination of groundwater, soil moisture, and other components. These GRACE datasets were widely applied for water balance studies on the basin scale (e.g., [25]), storage variations on the basin and sub-basin scale (e.g., [26–28]), estimation of the recharge and depletion rates of the aquifer (e.g., [29]), identification of the natural and human-fabricated influences on water availability and mass fluctuation [30], and calculation of the hydrological plus cryospheric excitation of polar motion [31]. Furthermore, some Middle Eastern studies have merged GRACE with other relevant climatic datasets to predict fluctuations in the amount of water stored underground and assess the behavior of the aquifer (e.g., [32–42]).

The GRACE Follow-On (GRACE-FO) mission was launched by NASA and GFZ as a continuation of the GRACE mission [43]. The initial GRACE project, which orbited the Earth from 2002 to 2017, was followed by this mission. It improves upon the accomplishments of its predecessor while also testing a new technology that greatly increases the measurement system's already impressive precision. It also contributes data to the high-resolution monthly global models of the Earth's gravitational field that were started during GRACE. The GRACE-FO twin satellites were sent from Germany to Vandenberg Air Force Base in California in December 2017, and a SpaceX Falcon-9 rocket launched them on 22 May 2018 from that location [44]. The Jet Propulsion Laboratory (JPL), the GFZ), and the Center for Space Research at the University of Texas (CSR), Austin are the three processing facilities that provide monthly gravity solutions for the GRACE and GRACE-FO Science Data System.

GRACE is unable to distinguish between contributions from TWS's various compartments (e.g., soil moisture, surface water, groundwater). To overcome this challenge, climate model outputs were integrated with GRACE data allowing separate individual components from GRACE-derived TWS estimates to be extracted and the data's horizontal resolution to be improved. Climate model outputs employ quantitative approaches to mimic the interactions of the atmosphere, seas, land surface, and ice, among other significant climate drivers. These models have several applications in climate prediction, water cycle modeling, and water resource management. One of these is the Global Land

Data Assimilation System (GLDAS; [45–47]). GLDAS collects observational data from satellites and ground stations. It calculates optimal fields of land surface states and fluxes using advanced land surface modeling and data assimilation techniques. Previous research in Saharan Africa [48] showed that GLDAS provides better accurate estimations of soil moisture in arid settings compared with other land surface models.

Other recent gravity field data from the Gravitational Models of the Earth have been utilized to look at crustal characteristics and features on a broad scale [49]. Groundwater investigation, subsurface geology [50,51], the shape of the magma chamber [52], and land subsidence [53] have all used aircraft and/or ground-based geophysical data on a smaller scale.

A previous investigation carried out by [54], using gravity data from GRACE, showed that the north-central part of the Middle East lost ~143.6 km^3 of total water storage between 2003 and 2009. By using data from land surface models, they showed that the groundwater depletion was 91.3 $\pm$ 10.9 km^3 in this region during 2003–2009, where a low rate of storage of 14.7 $\pm$ 9.3 km^3 was lost during 2003–2006, and a higher rate of 76.9 $\pm$ 10.1 km^3 was lost during the drought event (2007–2009). However, no previous studies on the calculation of groundwater storage changes for the entire country have been conducted in Iraq. Therefore, in this work, GRACE data were used in conjunction with GLDAS data to map the spatio-temporal and estimate the mass variations caused by climatic effects and/or groundwater withdrawal in Iraq. The time-variable gravity data were used to estimate the changes in the ΔTWS. To estimate groundwater storage variations (ΔGWS), the outputs of GLDAS model were used to exclude non-groundwater components from ΔTWS.

2. Geological and Hydrogeological Setting

The geology of Iraq is represented by a thick succession of marine and continental sediments overlying the basement rocks [55]. The Khabour Quartzite Formation of the Cambrian and Ordovician age represents partially the oldest rocks that are exposed on the surface of Iraq. Most of the deeper basement rocks were formed in the Proterozoic. Due to the Neo-Tethys extensional faulting, the northeastern part of the study area has a thinned quasi-continental crust [56]. The grabens were formed, then thick sediments accumulated. The deposition was paused in Late Silurian twice due to the Caledonian orogeny, and in the Carboniferous–Permian due to the Hercynian orogeny. The Kaskaskia marine transgression event resulted in the formation of the Devonian Pirispiki Red Beds and Chalki Volcanics along with the limestone and Ora Shale formations [57]. The Ga'ara and the Chia Zairi Limestone formations were formed during the Permian time. Northern Iraq is dominated by limestone, marl, evaporite, and shale, while interactions of calcareous and clastic rocks appear in the south. Central Iraq and the Mesopotamian Foredeep have thick sediments. The Maastrichtian and Paleocene sediments range from ~100 m to ~2.79 km. The basement faulting represents the orogeny period where the Zagros Mountains initiated form [56,58]. The geological map of Iraq is shown in Figure 1.

According to physiological, structural, geological, and hydrogeological properties, Iraq was categorized into seven zones from a hydrogeological standpoint by [59]. The hydrogeological and hydrochemical properties of each zone are distinct. These zones (Figure 2) are: The Mesopotamian Foredeep (Mesopotamian), Low and High Folded Zone, Suture and Thrust Zone, Al-Jazira Zone, and Western and Southern Desert Zones. While Ref. [60] categorized Iraq's groundwater aquifers system into five primary hydrogeological units: Foothill, Al-Jazira, Mandali-Badra-Teeb, Mesopotamian, and Desert Aquifer systems, which include two aquifers subsystem, the northern and southern. The hydraulic properties of groundwater-bearing layers show higher values in gravel and sandy fragment aquifers, as well as geological formations with a high intensity of fractures, fissures, and karstic gaps, and lower values in restricted clay layers or impermeable crystalline layers with no cracks and fissures [61].

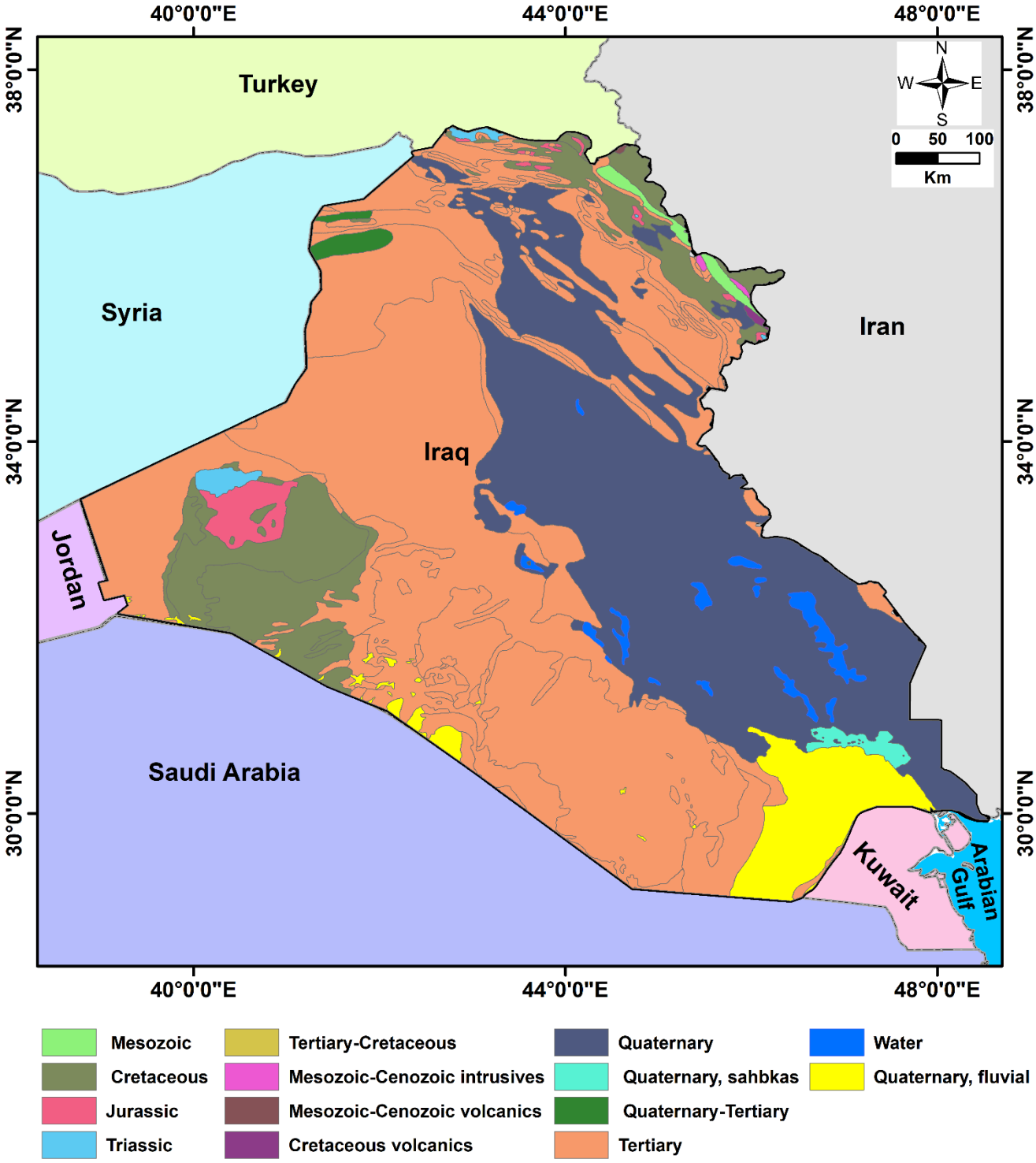

Figure 1. Geological map of Iraq.

Geological, structural, and lithological factors influence the spatial distribution and extensions of hydrogeological components, such as aquifers and aquitards, as well as their hydrological characteristics. In Iraq, fourteen major aquifers (Figure 3) have been identified and categorized by [60,62] based on the above-mentioned features and their link with the geological formations that store groundwater. The aquifer's components range from densely fractured and fissured limestone to karstified carbonate rocks, as well as sandy limestone, limestone, and sandstone. Gravel sands, karst limestone, gypsum, sandy deposits, and conglomerates are examples of other aquifer materials. According

to [61], the directions of groundwater flow in Iraq vary depending on the parameters of subsurface aquifers, such as hydraulic features, hydraulic slope, and the hydrogeological boundaries of the basins that contain these aquifers. The difference between the levels of groundwater in the aquifers and the inclination of the aquifers determines the flow of groundwater [63]. However, the general trend of the groundwater flow is towards the lowland of the Mesopotamian zone in the southeastern part of Iraq. The groundwater levels vary from higher values of about 550 m above mean sea level (amsl) close to the Foothill zone in the northeastern part and the Rutba subzone in the western part to about 0 amsl in the Mesopotamian zone (Figure 4; [60,64]).

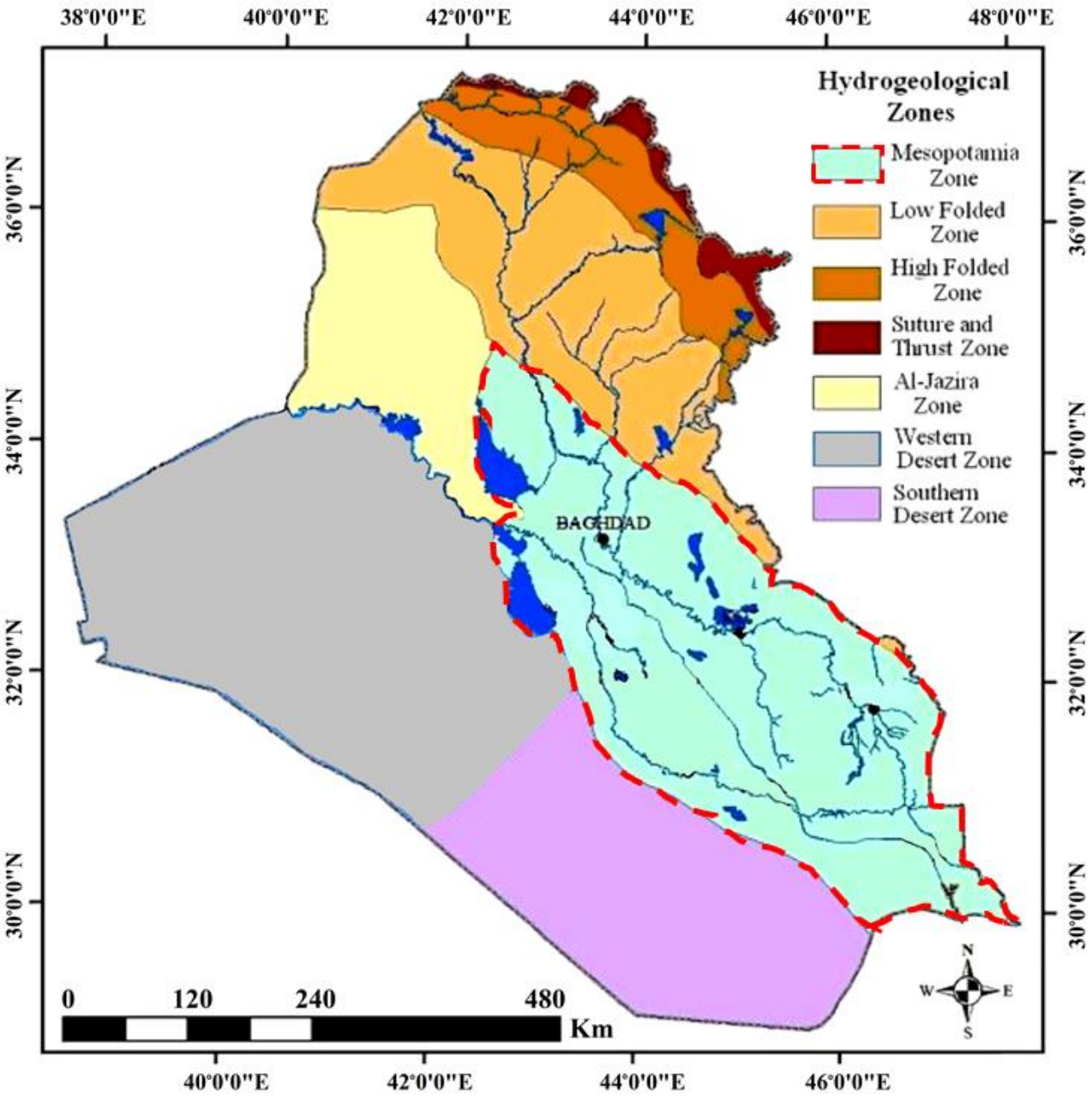

Figure 2. The main hydrogeological zones in Iraq (after [59]).

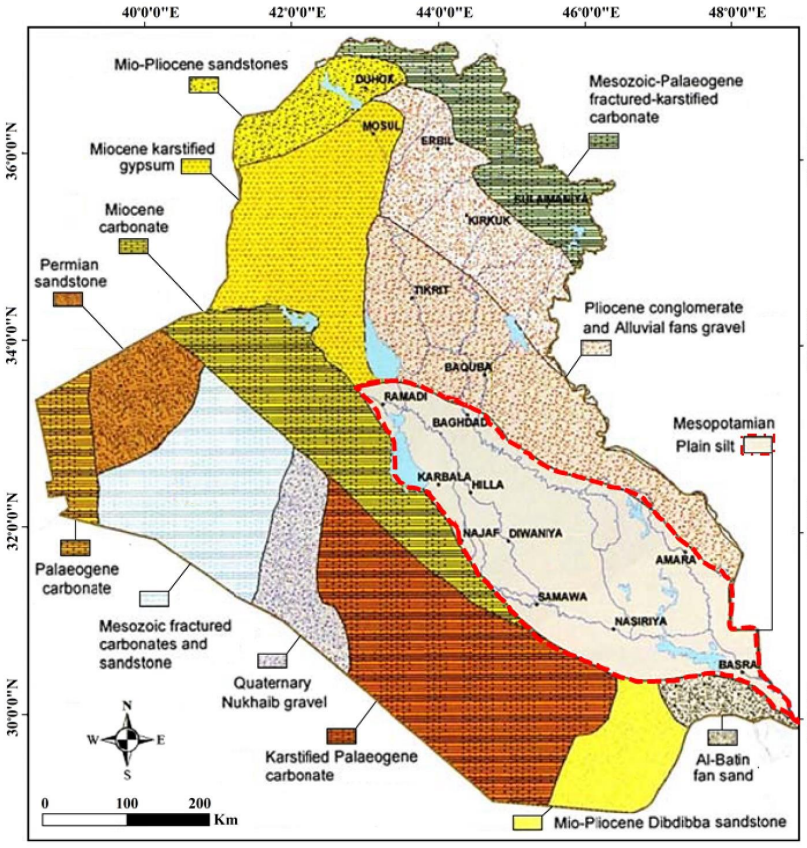

Figure 3. The major groundwater aquifers in Iraq (after [60,62]).

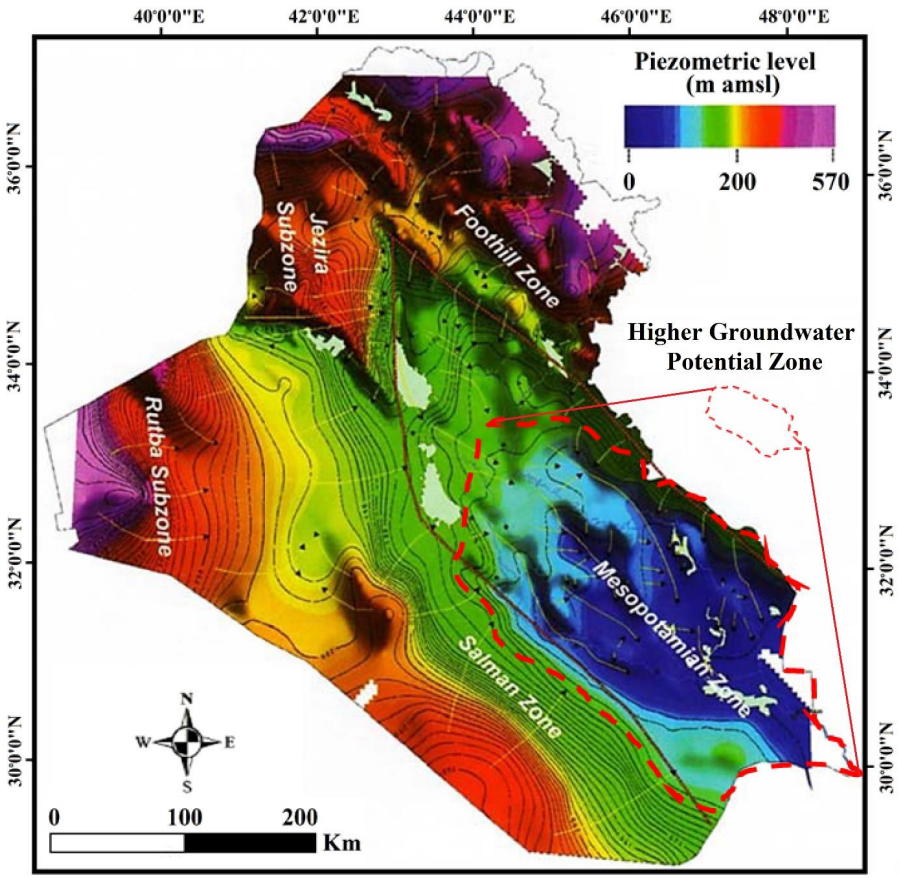

Figure 4. Groundwater levels in Iraq in m amsl (after [60,64]).

3. Data and Methodology

3.1. GRACE Data

Three time-variable gravity mascon solutions provided by GRACE processing centers were used in the current study. The mascon products are represented by JPL-RL06M v02, CSR-RL06M v02, and GSFC-RL06M v01 datasets from JPL, CSR, and the NASA Goddard Space Flight Center (GSFC), respectively. In comparison to spherical harmonic solutions, these mascon solutions capture all signals within the GRACE noise levels with improved spatial resolution and lower error. No de-striping, and/or smoothing is required. The scaling factor might also be not required for these products [43,65–67].

TWS anomalies were calculated for each equal-area 3° × 3° spherical cap mascon block in the JPL-RL06M v02 solution [43,67]. The TWS fluctuations are sampled to 0.5° × 0.5° longitude–latitude grids in the final dataset. Provided that the JPL-RL06M v02 has a real 3° resolution, the scaling factors provided by JPL must apply to recover the leakage signals caused by 3° mascon blocks. JPL-RL06M v02 data provide enhanced separation of land and ocean mascons compared with the prior version (JPL-RL05M). As a post-processing step, the Coastal Resolution Improvement filter was used for the entire mascon solution to detect land and ocean mass from individual mascons that cross coastlines [43] and to reduce leakage errors across coastlines [67].

TWS fluctuations are displayed in 0.25° by 0.25° longitude–latitude grids in the CSR-RL06M v02 solution, which was calculated from an equal area with a 1° resolution [66,68]. In this new grid, the hexagonal tiles that make up the shoreline are divided into ocean and land tiles to minimize signal leakage between the two. For these small mascons, the scaling factor is not necessary. The GSFC-RL06v1.0 mascon solution was calculated for each 0.5° equal-area square mascon was utilized in addition to the JPL and CSR mascon datasets.

The cubic-spine approach was used to interpolate the missing monthly data. The mascon solutions, throughout the investigated period, were utilized in the current study. To obtain the best-fit line for a set of points, the slope values of the TWS trends were determined using the least squares fitting method using Equation (1). After then, the errors associated with the obtained trend values were calculated.

$$Slope = \frac{\sum(y - \overline{y})(x - \overline{x})}{\sum(x - \overline{x})^2} \quad (1)$$

Given (x_1, y_1), (x_2, y_2), . . . , (x_n, y_n) are the data points, the y is the dependent variable, and $\overline{y}$ stands for the average. The independent variable is x and their average is $\overline{x}$.

3.2. GLDAS and TRMM Data

Due to the scarcity and unavailability of data from gauge stations across the research area and because GRACE cannot differentiate between anomalies caused by different TWS components, two GLDAS [45] models (CLM, VIC, and NOAH) were employed to estimate the non-groundwater components. These components were used to differentiate the ΔTWS into its main components (e.g., soil moisture, canopy water storage, and snow water equivalent). The GLDAS data span the same period as GRACE data. Because there is a scarcity of rainfall data from ground stations, we used data from the satellite Tropical Rainfall Measuring Mission (TRMM) to create the average monthly rainfall time series and the average annual precipitation (AAP). By averaging all the monthly rainfall data over a year, the AAP rate was obtained. It was utilized to investigate the impact of precipitation on GWS over the course period of the study.

3.3. Temporal Variations in Surface Water Storage

Lake Tharthar is the largest lake in Iraq. Its water body has an impact on GRACE data-based mass variations and, as a result, GWS calculations. The global reservoir and lake monitoring database of the United States Department of Agriculture's Foreign Agricultural Service (USDA-FAS) was used to construct the time series of Lake Tharthar's surface water (GRLM). In the research region, the trend of surface water storage fluctuations was

determined. The area and surface water level of Lake Tharthar over the study region were used to estimate the temporal mass variation in the lake over the studied period. Because it does not contribute to the GWS, the trend of the lake's surface water storage variation was subtracted from the TWS.

Using Equation (2), which has been used by several scientists (e.g., [33,35,46,69–73]), the trend value in groundwater storage variation was calculated from the terrestrial water storage variations by removing other derived terrestrial storage changes from GLDAS data [33,46,74] and the variations in surface water storage.

$$\Delta TWS = \Delta GWS + \Delta SMS + \Delta SWS + \Delta CWS + \Delta SWE \quad (2)$$

where ΔTWS and ΔGWS refer to the changes in terrestrial water and groundwater storage, respectively. ΔSWE, ΔCWS, ΔSWS, and ΔSMS, indicate snow water equivalent, canopy water storage, change in surface water, and soil moisture, respectively.

4. Results

The analysis of TRMM-derived rainfall data is shown in Figures 5 and 6. The study area received average annual precipitation of 223.4 mm/y for the whole investigated period. In the northeastern parts of Iraq, the AAP exhibits higher values of ~600−900 mm/y, close to the borders with Turkey and Iran (Figure 6) and decreases west and southwards, reaching lower values of ~70 mm/y, close to the borders with Jordan and Saudi Arabia. Three distinct climatic periods with unique AAPs were found. The results of the spatial distribution and the temporal variation in the secular trend in GRACE-estimated ΔTWS data are shown in Figures 7 and 8, respectively. The GRACE-estimated ΔTWS shows a depletion trend of -5.51 ± 0.68 mm/y (Table 1) for the averaging of the different solutions across the entire study area. The results of the decomposition of the ΔTWS were shown in Table 1 using outputs of the GLDAS models and the trend value of Lake Tharthar's surface water storage variation. The monthly ΔGWS time series (Table 1) shows a negative trend estimated at -4.86 ± 0.69 mm/y during the entire period.

Table 1. TWS trends values and components (mm/y) were calculated by GRACE and GLDAS.

Component		Entire Period	Period I	Period II	Period III
GRACE total (ΔTWS)	CSR-M	-5.79 ± 0.70	$+6.43 \pm 4.08$	-5.60 ± 1.24	$+32.7 \pm 13.07$
	JPL-M	-5.11 ± 0.70	$+7.15 \pm 4.00$	-5.22 ± 1.18	$+30.16 \pm 12.25$
	GSFC	-5.64 ± 0.67	$+6.87 \pm 3.97$	-7.77 ± 1.15	$+22.89 \pm 13.5$
	AVG	-5.51 ± 0.68	$+6.82 \pm 1.92$	-6.20 ± 1.17	$+28.58 \pm 12.78$
ΔSMS		-0.03 ± 0.02	$+0.01 \pm 0.01$	$+0.08 \pm 0.04$	-0.84 ± 1.45
Tharthar Lake		-0.62 ± 0.06	$+9.28 \pm 0.93$	-2.48 ± 0.25	$+34.05 \pm 3.4$
ΔGWS		-4.86 ± 0.68	-2.47 ± 2.20	-3.79 ± 1.20	-4.63 ± 12.99
p-value		<0.0001	0.0542	<0.0001	0.0253
AAP		223.4	252.5	194.2	311.6

CSR-M and JPL-M: mascon products; JPL-SH and CSR-SH: spherical harmonic solutions; TWS: Changes in Terrestrial Water Storage; GWS: groundwater storage change; SWE: change in snow water equivalent; SMS: change in soil moisture; CWS: change in canopy water storage; SWS: changes in surface water storage; AAP: annual average precipitation. *p*-value is the probability value.

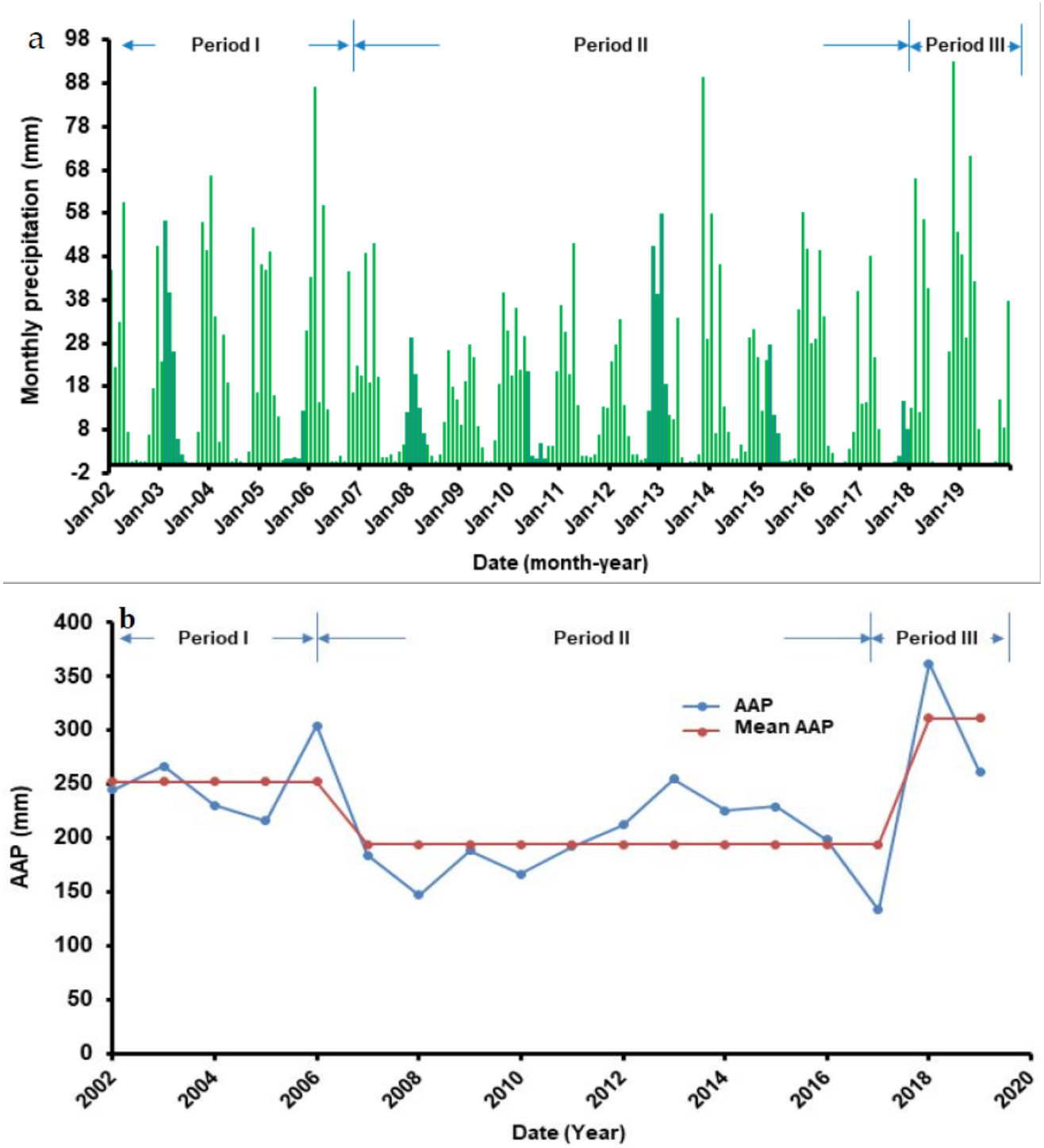

Figure 5. Monthly rainfall (**a**) and the AAP (**b**) over the study region during the three periods.

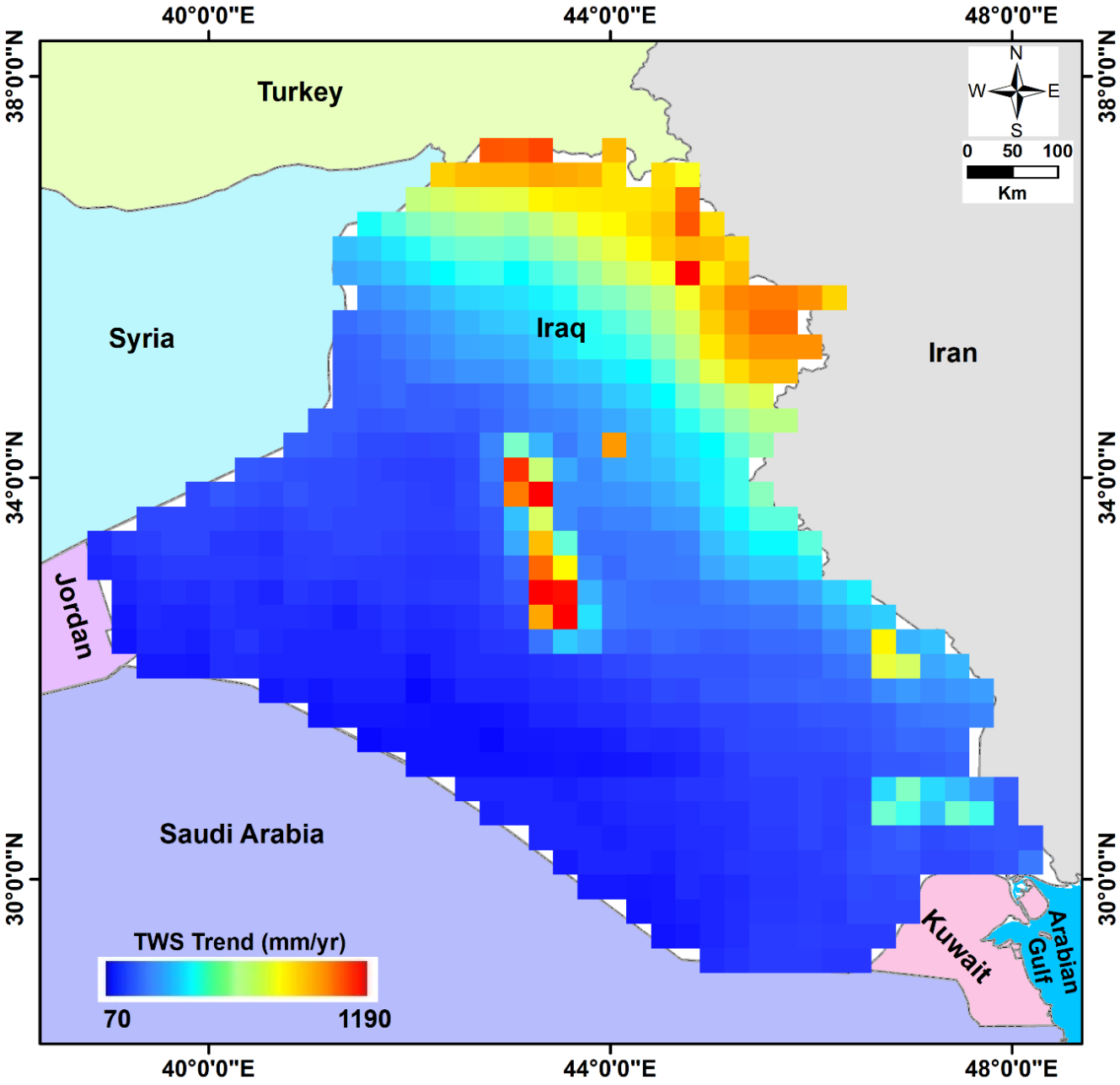

Figure 6. AAP (mm) was taken from TRMM data over the study area.

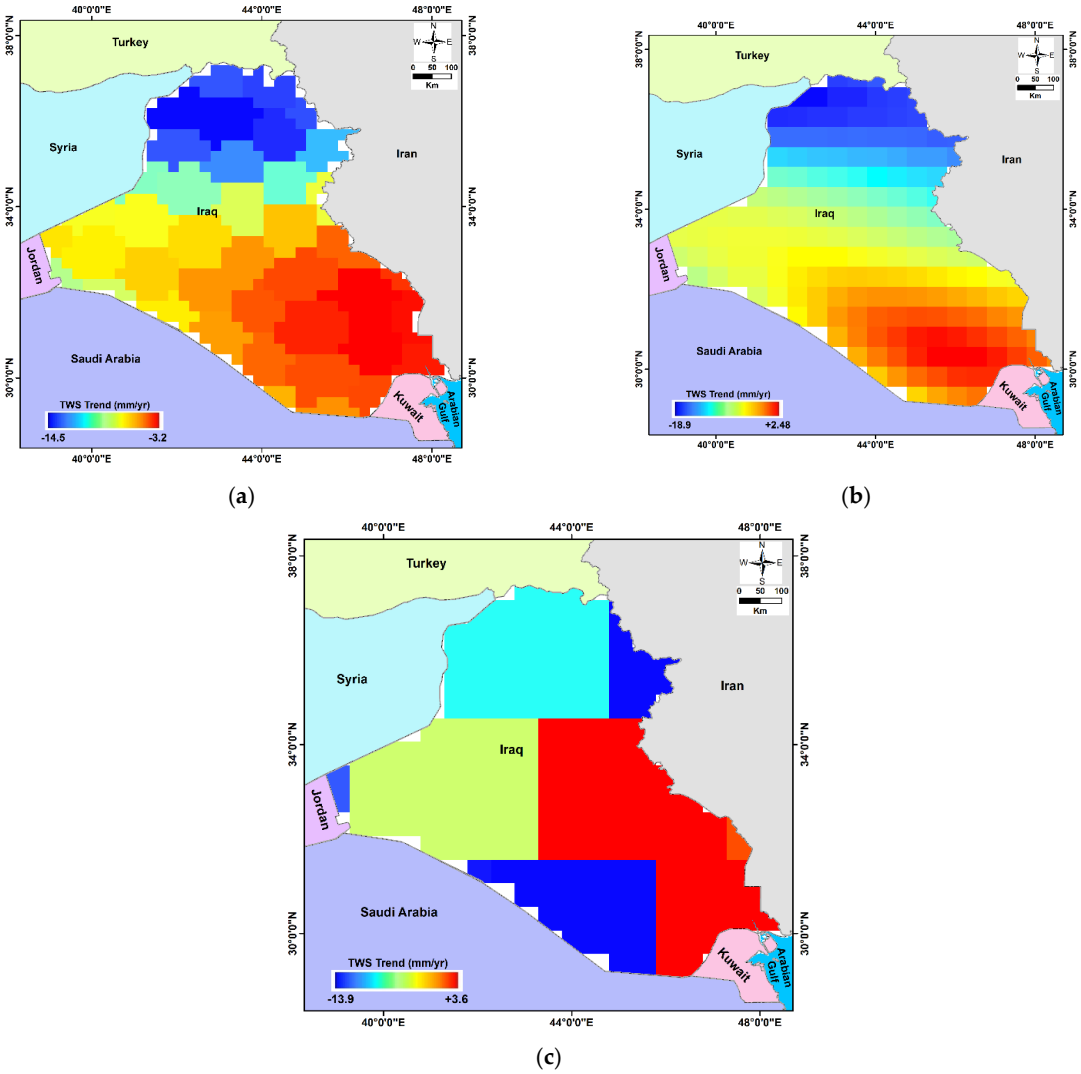

Figure 7. Average of the monthly CSR (**a**), GSFC (**b**), and JPL (**c**) products over Iraq produced a color-coded secular extracted TWS trend map during the entire period.

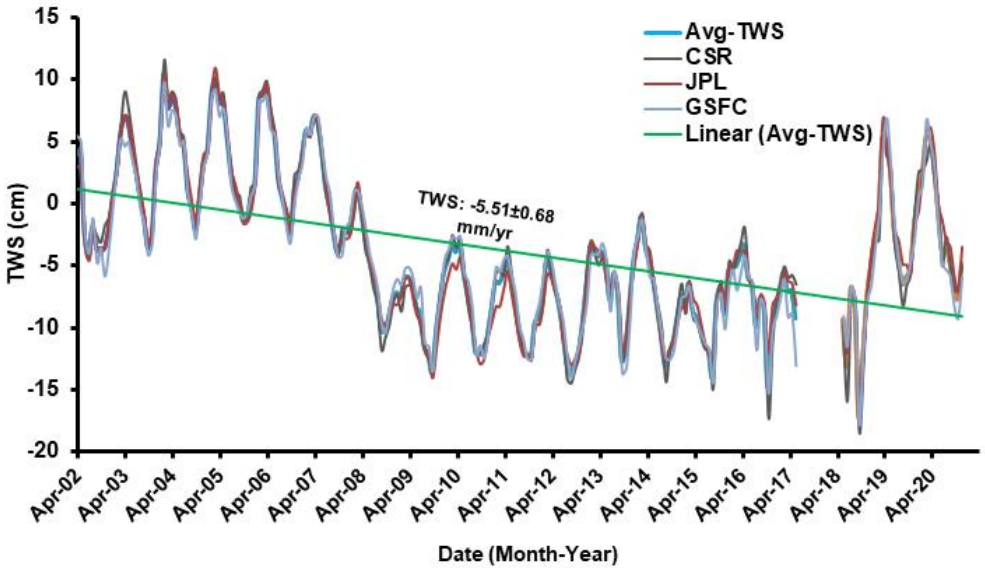

Figure 8. Monthly CSR, JPL, and GSFC mascon solutions and their averaging (Avg-TWS) for terrestrial water storage fluctuation over Iraq.

5. Discussion

5.1. Identification of Time-Periods

The climate data were used to identify three periods throughout the investigated time. Large changes occurred in 2007 as a result of the commencement of a drought and a rise in temperatures [75]. The three periods are discussed as follows: Period I covers the time preceding the onset of the 2007 drought, and Period II covers the time following its onset in 2007 until December 2017 as shown in Figure 5 which displays the measured mean monthly rainfall's temporal fluctuations. It indicates slightly higher average precipitation between April 2002 and December 2006, defining the first period (Period I); and lower values between January 2007 and December 2017, establishing the second period (Period II) of the investigated time in Iraq. It also shows a higher precipitation rate during the period between January 2018 and December 2020, characterizing Period III. The AAP rate shows that Period I (04/2002–12/2006) had a higher AAP rate of 252.5.1 mm/y; while period II (01/2007–12/2017) had a lower AAP rate of 194.2 mm/y; whereas Period III (01/2018–12/2020) had the highest AAP rate of 311.6 mm/y. The study area is receiving an average AAP rate of 223.4 mm/y over the entire study period (Table 1).

5.2. Water Budget

Figure 8 shows the spatial distributions of the secular trends in GRACE-derived ΔTWS from the monthly spherical harmonic and mascon solutions through the investigated period over Iraq. Inspection of this figure shows that the TWS is witnessing negative trend values increasing toward the south, close to the borders with Saudi Arabia and Kuwait, and decreasing toward the north. GRACE-extracted ΔTWS data were used to create time series for the study area. The ΔTWS trends extracted from the three different solutions indicate an overall depletion rate (Figure 8). The GRACE-derived ΔTWS estimated from CSR mascon, JPL mascon, and GSFC mascon witnessed depletion rates of -5.79 ± 0.70, -5.11 ± 0.70, -5.64 ± 0.67 mm/y, respectively. The TWS of the three different solutions are averaged at -5.51 ± 0.68 mm/y (Figure 8; Table 1) across the entire study area. Between the different TWS time series, there was a significant correlation ranging from 0.97 to 0.98 (Figure 9). The average ΔTWS time series shows three distinct trends of varying slope values during the whole investigated period, according to the linear regression analysis of their averaging (Figure 10), which are compatible with those identified based on the rainfall data (Figure 5). Examination of Figure 10 and Table 1 shows that the country experienced a TWS increase during Period I at $+6.82 \pm 1.92$ mm/y and a TWS decline at -6.20 ± 1.17 during Period II, and a much higher rate during Period III at $+28.58 \pm 12.78$ mm/y.

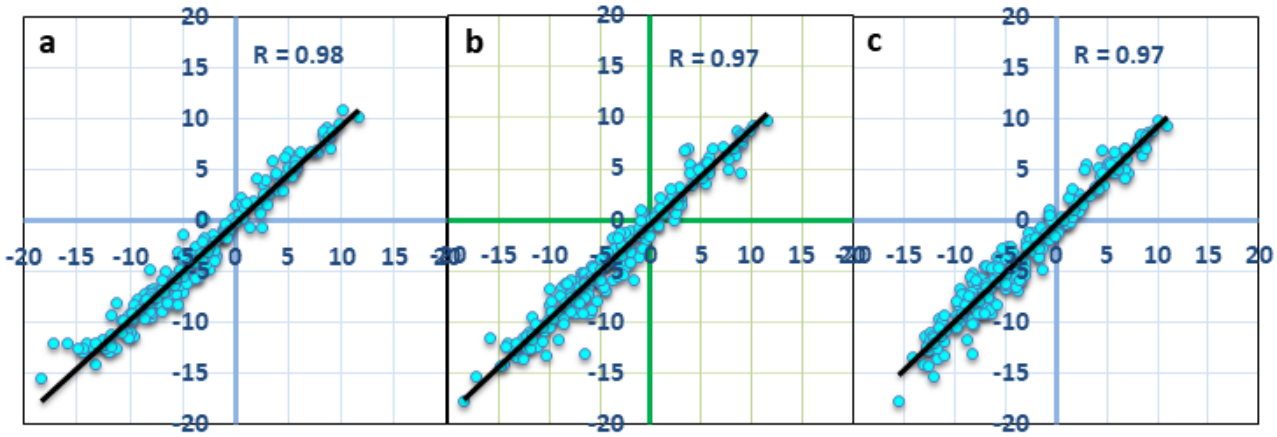

Figure 9. Correlation coefficients (R) between ΔTWS data from the averaging of JPL and CSR mascon solutions (**a**); CSR and GSFC mascon solutions (**b**); JPL and GSFC mascon solutions (**c**) over Iraq throughout the entire period.

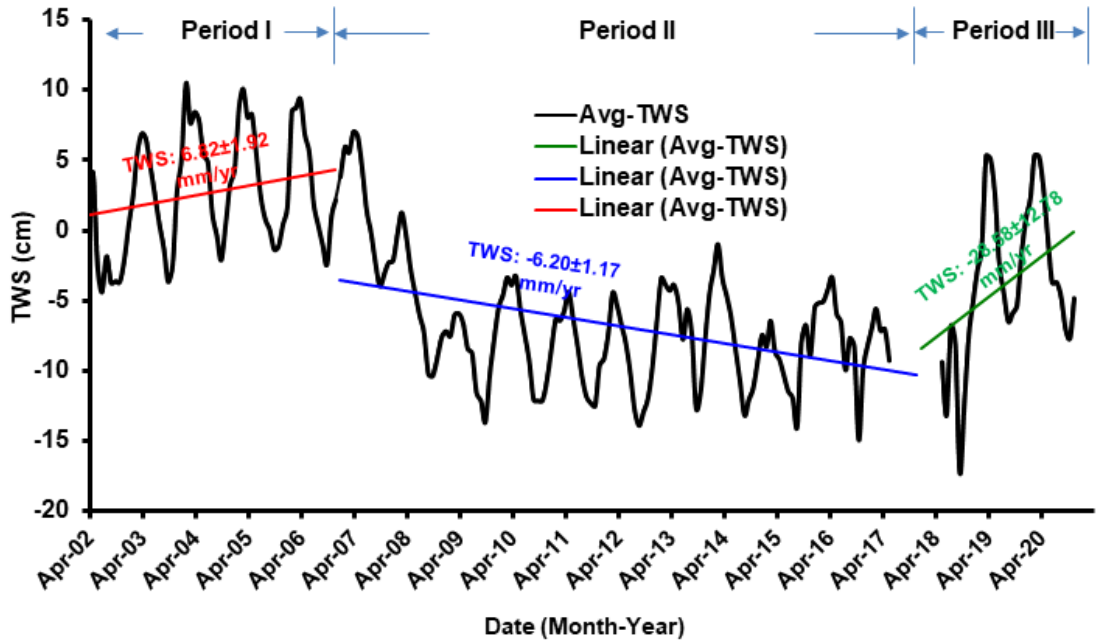

Figure 10. Time series for the Avg-TWS over Iraq during the three periods.

Over the study area, three GLDAS (CLM, VIC, and NOAH models) versions were utilized to calculate the differences in soil moisture storage (ΔSMS) (Table 1). The study area is experienced a slightly negative ΔSMS trend value calculated at +0.03 ± 0.01 mm/y (Figure 11) during the whole study period. During periods I and II, the ΔSMS trend was estimated to be +0.01 ± 0.01 and +0.08 ± 0.04, respectively (Table 1). However, during Period III, the ΔSMS trend was calculated to be −0.84 ± 1.45 mm/y (Table 1). Due to the lack of any observable trends in time series, the additional non-groundwater components represented by changes in canopy water storage (CWS), surface water storage (SWS), and snow water equivalent (SWE) are negligible in this arid environment.

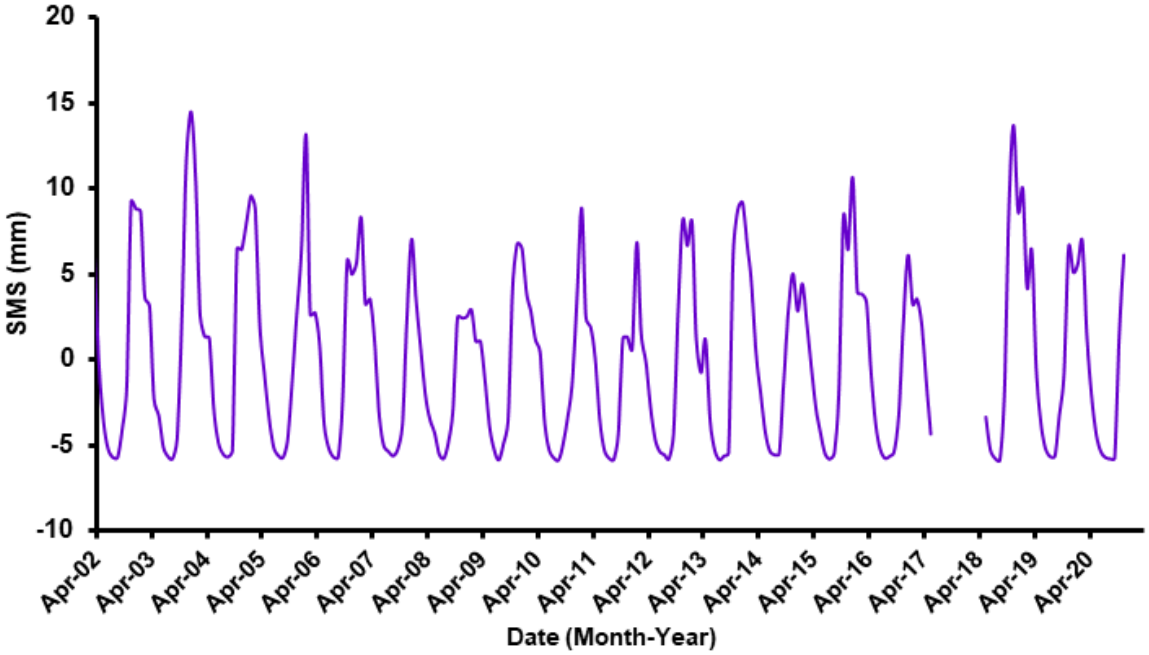

Figure 11. GLDAS-derived SMS over Iraq throughout the entire period.

Figure 12 exhibits the changes in Lake Tharthar's water level across the study period. It varied between a higher value of 54.4 m in 2004, a lower value of 43.7 m in 2018, and a maximum value of 55.8 m in 2019. The water level shows a rapid decrease, with the onset of the 2007 drought, from 52.0 m in 2007 to 45.2 m in 2009, and continues with small downward fluctuations until the year 2018. The lake's water level increased rapidly from the lowest value of 43.7 m in 2018 to 55.8 m in 2019, in response to the heavy rainfall rate occurring during 2019–2020. The water level of the lake was likely affected by the 2007 drought and groundwater depletion. The annual mass variation in the lake's water (Figure 13) was estimated. It has been subjected to a mass depletion of -0.27 ± 0.03 km^3/y. In the case of lake water level, there is a 10% margin of error. The lake has a surface area of 2710 km^2. When the mass loss is averaged over the full study area, the regional depletion rate is -0.62 ± 0.06 mm/y (Table 1) for the entire study period. Higher average precipitation rates in Period I, which ranged from 244.86 mm in 2002 to 304.23 mm in 2004, influenced the lake's water level, which varied from 45.43 m in 2002 to 54.44 m in 2004. Lower precipitation during the onset of the 2007 drought resulted in a large loss of the water surface area of the lake, causing a decrease in its water level from 52 m in 2007 to 43.7 m in 2018. This decrease in water level may be identical to that calculated by [35,76] for Lake Urmia in Iran which is subjected to the same climatic conditions. According to piecewise linear trend analysis, the lake gained around $+4.05 \pm 0.41$ km^3/y of water during Period I, which equals $+9.28 \pm 0.93$ mm/y over the entire area. During Period II, the lake volume depleted at a rate of -1.08 ± 0.11 km^3/y, averaging at -2.48 ± 0.25 mm/y across the entire region, owing to the commencement of the drought. The water volume in the lake rapidly increased at $+14.86 \pm 1.49$ km^3/y during Period III, which averaged at $+34.05 \pm 3.4$ mm/y across the entire country.

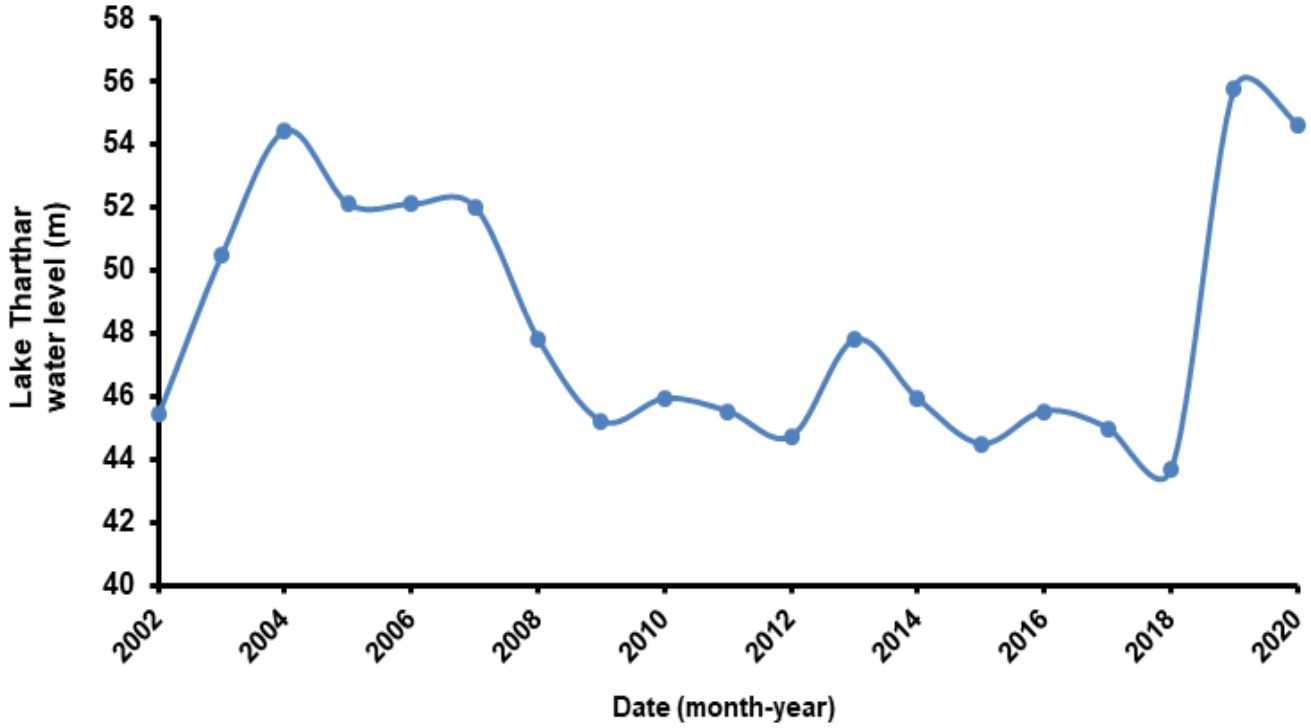

Figure 12. Time series of Lake Tharthar's water level throughout the entire investigated period.

Depletion rates of the total freshwater storage (ΔTWS) vary from -5.79 ± 0.70 to -5.11 ± 0.70 mm/y (Table 1) based on the three different solutions with an average value estimated to be -5.51 ± 0.68 mm/y across Iraq throughout the entire study period (Table 1). We subtracted the ΔSMS (-0.03 ± 0.02 mm/y) trend value as well as the Lake Tharthar trend (-0.62 ± 0.06 mm/y) from the ΔTWS trend, the GWS depletion was then calculated at -4.86 ± 0.68 (Table 1) during the entire investigated period.

Groundwater depletion was 17.3 ± 2.1 mm/y in the transboundary portions of the Euphrates and Tigris River basins, as well as the west part of Iran, from 2003 to 2009. Iran, which has similar climatic conditions to the study area, had an overall groundwater depletion of −10.28 ± 0.73% between 2002 and 2016 [35].

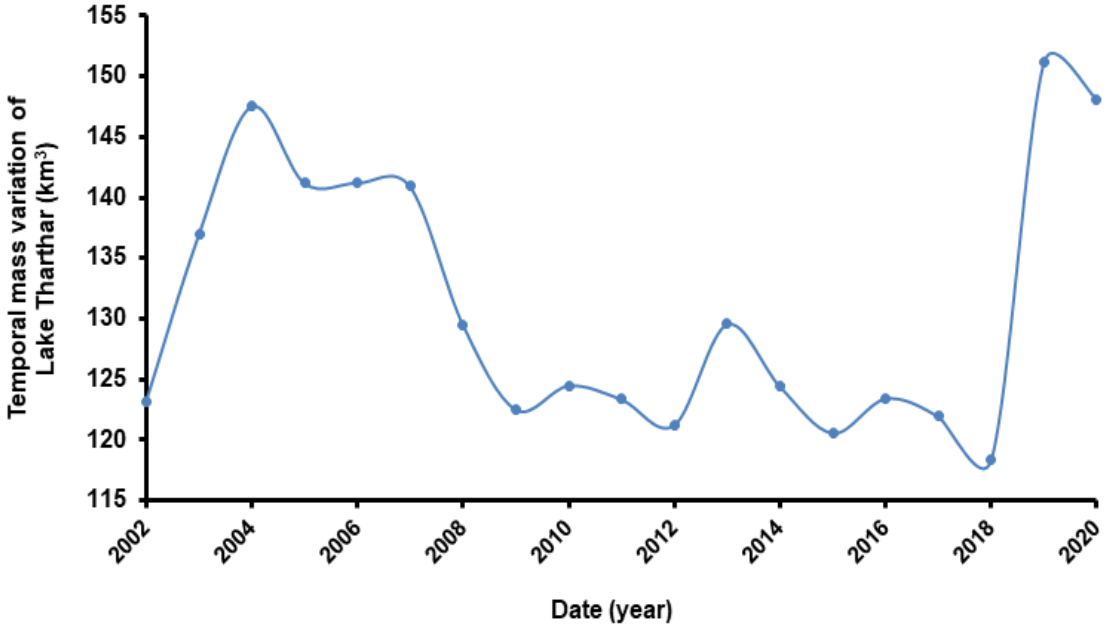

Figure 13. The annual mass variation in Lake Tharthar throughout the entire investigated period.

The ΔGWS time series (Figure 14) exhibits slightly similar changes to the ΔTWS time series (Figure 8) while having different trend values. By excluding the values of the ΔSMS (+0.01 ± 0.01 mm/y), the approximated value of the GWS for Period I is +6.81 ± 1.92 mm/y (Figure 15). However, the ΔGWS decreased to −2.47 ± 2.20 mm/y (Table 1) by subtracting Lake Tharthar's trend value (+9.28 ± 0.93 mm/y) from the ΔTWS trend value.

By subtracting the values of the SMS (+0.08 ± 0.04 mm/y) and Lake Tharthar's (2.48 ± 0.25 mm/y) trend values from the ΔTWS trend value, ΔGWS reveals a depletion trend of −3.79 ± 1.20 mm/y during Period II (Table 1). The GWS displays a high depletion rate estimated to be −6.81 ± 1.19 mm/y during Period II without subtracting the trend of Lake Tharthar. Heavy rainfall resulted in a quick rise in the water level of Lake Tharthar; therefore, the TWS exhibits a substantially higher trend value of +28.58 ± 12.78 mm/y during Period III. After subtracting the SMS (−0.84 ± 1.45 mm/y) during Period III, the estimated ΔGWS trend was found to be +29.42 ± 12.86 mm/y (Figure 15); however, after removing the lake's trend value (+34.05 ± 3.4), it decreased to −4.63 ± 12.99 mm/y (Table 1).

Throughout the whole study period, the study area displayed a general negative GWS trend. Keeping the periods in mind, the GWS decreased from −2.47 ± 2.20 mm/y in Period I to −3.79 ± 1.20 mm/y in Period II. This drop in Period II is mostly related to man-fabricated activities as well as the declining trend in rainfall that began with the start of the 2007 drought and continued to 2017. Despite the study area experiencing higher rainfall rates in 2019–2020, the GWS trend still declined, reaching −4.63 ± 12.99 mm/y over Period III. The significant groundwater loss and surface runoff into the small Mesopotamian plain zone and the Euphrates and Tigris Rivers may have been the source of this over the entire study area.

Iraq is one of the nations in the world that is most at risk from drought, climate change, and rising desertification rates. Due to this, desertification rates in southern Iraq have grown. Any wind intensity allows light soil and mud particles to move due to the drying of these areas, which increases the frequency of dust storms over Iraq and the Gulf region.

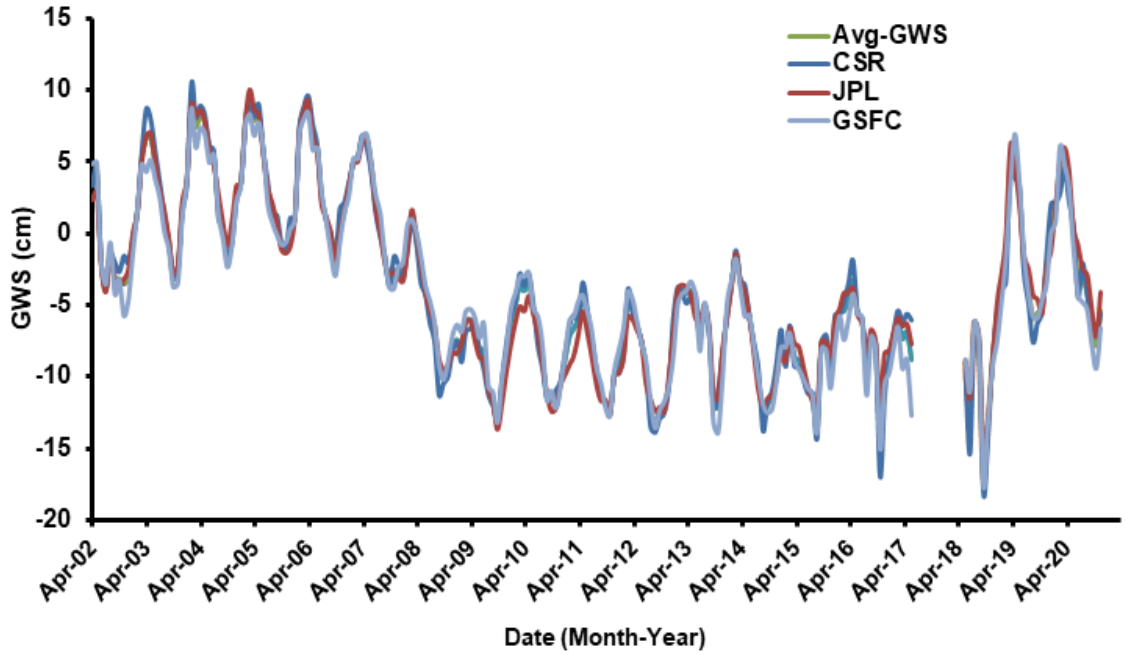

Figure 14. Monthly CSR, JPL, and GSFC mascon solutions for GWS fluctuation and their averaging (Avg-GWS) over Iraq after removing the SMS trend value from the TWS trend value.

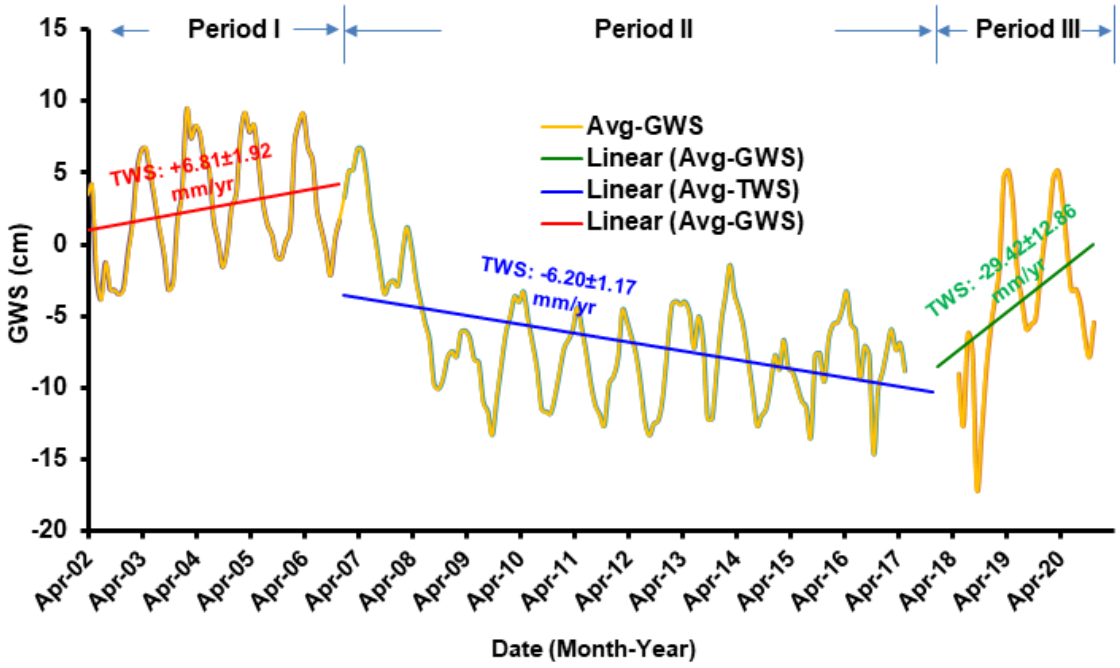

Figure 15. Time series for the Avg-GWS across the study area over the three periods after subtracting the SMS trend value.

5.3. Stream Networks

The research area's surface elevation map, created using the ETOPO1 Global Relief Model, is shown in Figure 16. There is a sizable relief, ranging from 700 to 3000 m, across its northern mountainous region. However, the western part of the region presents a moderate relief of roughly 600–900 m close to the Jordanian border. The western and northeastern parts of Iraq come together to create streams that feed the Mesopotamian plain downstream of the Tigris and Euphrates Rivers. Surface runoff creates streams that flow toward the Tigris River under the assumption that a significant precipitation rate (Figure 16) occurs

over the northern mountainous region along the borders with Iran and Turkey. The stream networks and the positive TWS signals from GRACE (Figure 7) show that streams and rivers fed the Mesopotamian plain throughout the whole period.

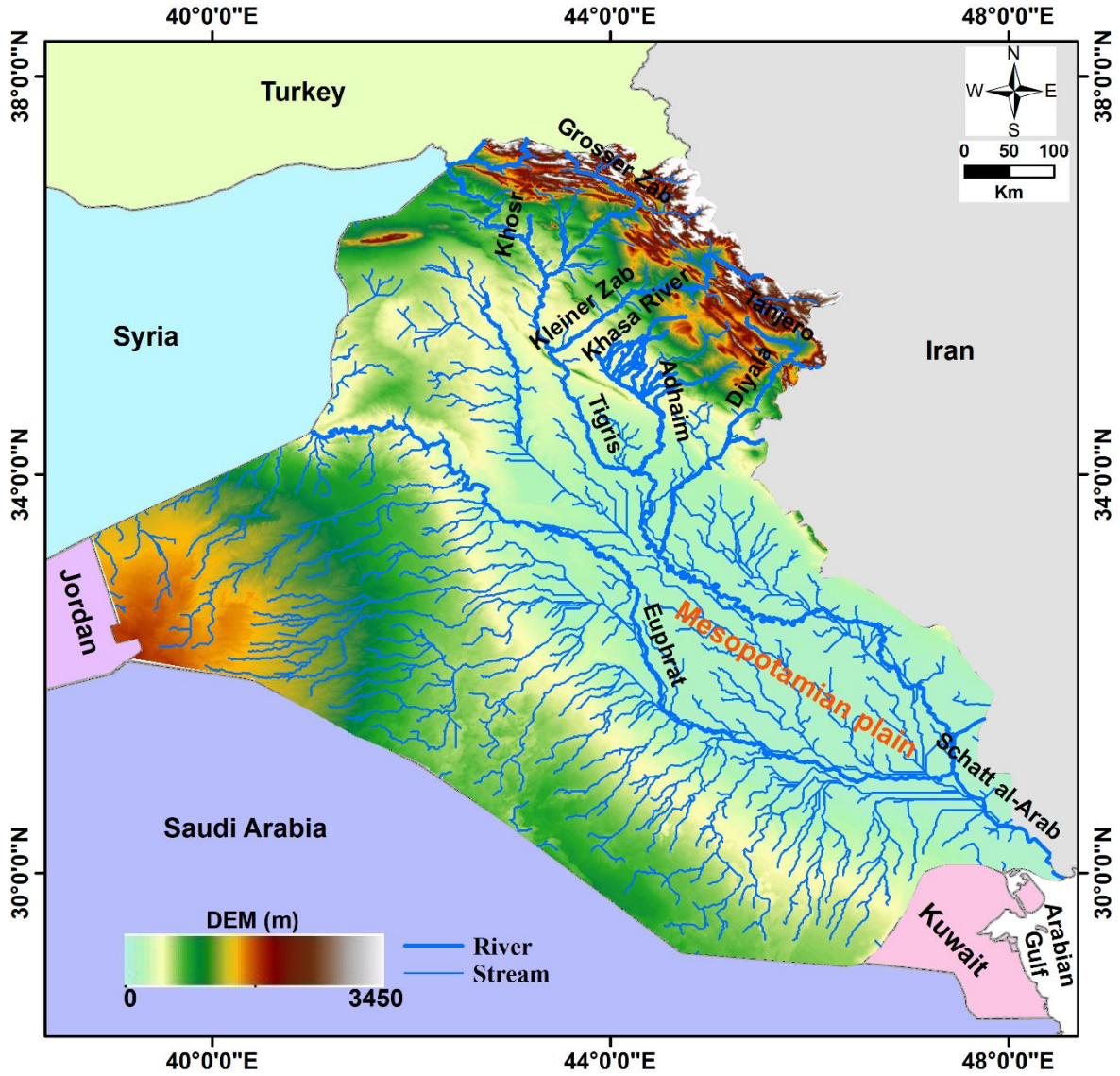

Figure 16. A map of the study area shows the ground surface elevation using a DEM; additionally, it displays the local stream networks.

5.4. Sediment Thickness

The NOAA National Geophysical Data Center's website provided the sediment thickness information [77]. The northeastern portion of Iraq has a very low sedimentary success varying from 0 up to 1200 m over the mountainous region, dissected by wadies, which drain the surface runoff toward the rivers and the Mesopotamian plain to the south. The western region shows sedimentary succession varying from 1800 to about 3000 m (Figure 17). The sedimentary succession shows values varying from ~6000 m in the southwestern region to more than 9000 m in the southeastern part of the Mesopotamian plain. This can support the occurrence of a high reserve of the fluid downstream of the rivers, as indicated by the positive TWS signals over this region.

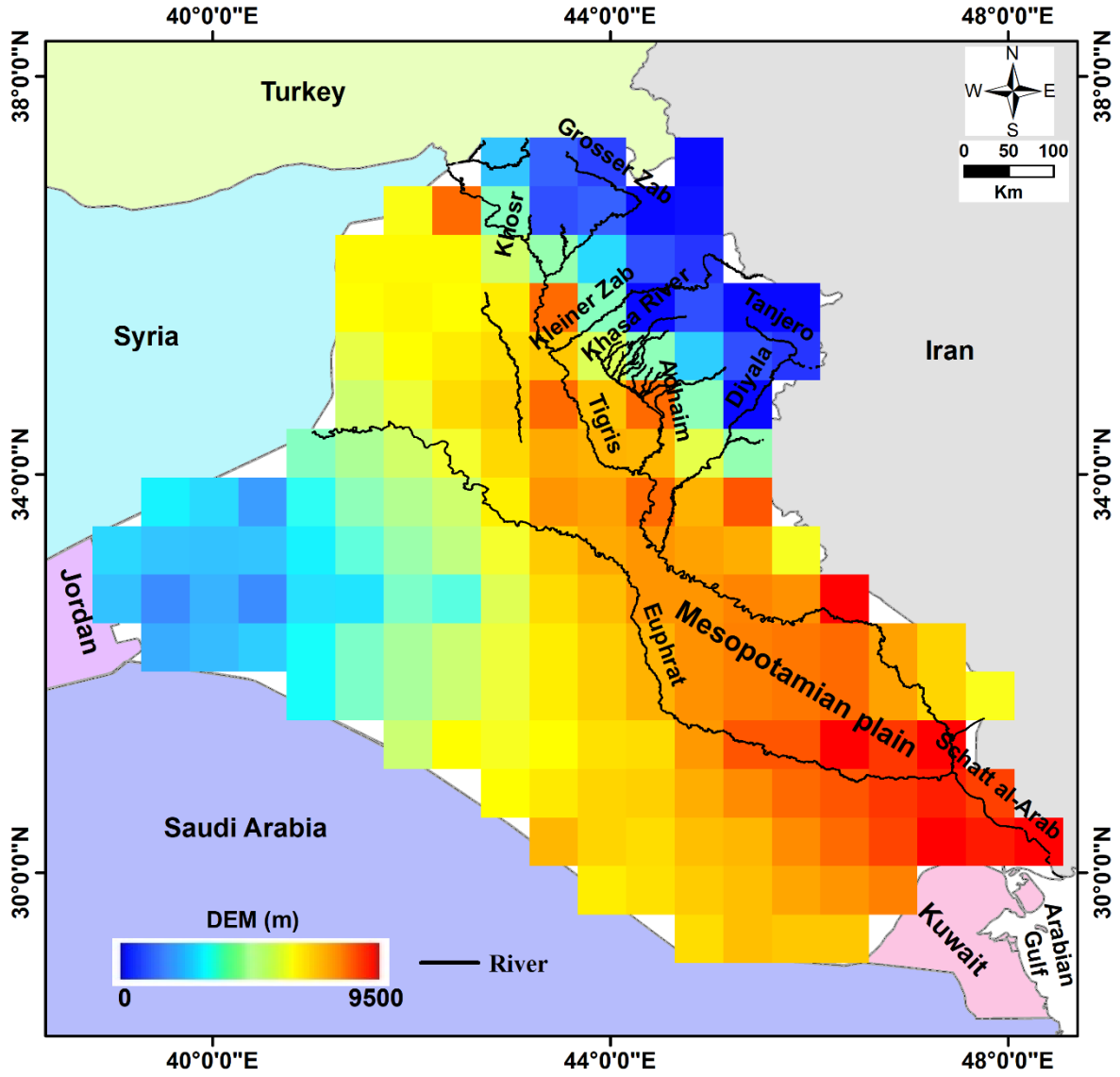

Figure 17. A sediment thickness map showing thickness of the sedimentary succession (m).

5.5. Level of Confidence and Inaccuracy Estimation in GWS Trends

In regions where this phenomenon is considerable, errors in GRACE data are caused by observations, spatial and spectral leakages, post-processing, and glacial isostatic adjustment (GIA). The computed ΔGWS trend data were analyzed using a Student t-test. At a 95% confidence level, the t value is used in conjunction with a confidence chart to calculate the probability (*p*-value) and statistically significant trends. The ΔGWS trend has an extremely low *p*-value (0.0001), indicating a significant trend at a confidence level of >95%.

$$\sigma_{GWS} = \sqrt{\{(\sigma_{TWS})^2 + (\sigma_{SMS})^2 + (\sigma_{SWS})^2\}} \quad (3)$$

As a result of the errors (Table 1) calculated with TWS (σ_{TWS}), SMS (σ_{SMS}), SWS (σ_{SWS}), CWS (σ_{CWS}), and SWE (σ_{SWE}), the error (σ_{GWS}) in GWS was established using Equation (3).

Errors on trend estimates of the GRACE-derived GWS were determined to be equal to 0.68 mm/y for a trend of 4.86 mm/y from April 2002 to December 2020.

6. Conclusions

Iraq experienced groundwater loss from April 2002 to December 2020, according to our findings:

- Based on rainfall studies in Iraq, three distinct climatic periods were identified over the study period: Period I (12/2002–12/2006), which had a higher precipitation value of 252.5 mm/y; Period II (01/2007–12/2017), which had a lower precipitation value of 194.2 mm/y; and Period III (01/2018–12/2020) with the maximum precipitation rate of 311.6 mm/y;
- During the whole study period, the GRACE-derived TWS showed a general depletion pattern, with positive TWS signals over the southern part of the country and negative signals over the northern parts;
- Following the drought and the lower rainfall period starting in 2007, Iraq's groundwater declined;
- For Period I, the rate of GWS was calculated to be -2.47 ± 2.20 mm/y; for Period II, a higher GWS depletion rate of -3.79 ± 1.20 mm/y was obtained than for Period III;
- The GWS indicates an overall depletion rate of -4.63 ± 12.99 mm/y over the study area throughout the period studied, which is the result of major anthropogenic activity combined with the low rainfall rate that prevailed in the majority of Iraq;
- The Euphrates–Tigris Rivers and the Mesopotamian plain, which has a larger sediment thickness, receive surface water from the streams that cross the mountainous areas of northeastern Iraq;
- The findings demonstrate that the GRACE and GLDAS datasets are capable of providing a reliable calculation of the water budget in arid environments.

Author Contributions: Conceptualization, A.M.; Data curation, A.O., A.A. and A.M.; Formal analysis, A.A.; Investigation, A.O., A.A. and A.M.; Methodology, A.O. and A.M.; Project administration, A.M.; Resources, A.O., A.A. and A.M.; Software, A.M.; Validation, A.A.; Visualization, A.A. and A.M.; Writing—original draft, A.O. and A.M.; Writing—review & editing, A.M. All authors have read and agreed to the published version of the manuscript.

Funding: This research received no external funding.

Data Availability Statement: The data is available upon request from the authors.

Conflicts of Interest: The authors declare that there is no conflict of interest.

References

1. United Nations, Department of Economic and Social Affairs. *Population Division (2013)*; United Nations: New York, NY, USA, 2013.
2. Bernauer, T.; Böhmelt, T. International conflict and cooperation over freshwater resources. *Nat. Sustain.* **2020**, *3*, 350–356. [CrossRef]
3. Wada, Y.; van Bee, K.L.P.H.; van Kempen, C.M.; Reckman, J.W.T.M.; Vasak, S.; Bierkens, M.F.P. Global depletion of groundwater resources. *Geophys. Res. Lett.* **2010**, *37*, L20402. [CrossRef]
4. United Nations World Water Assessment Programme (WWAP). The United Nations World Water Development Report 2014. In *Water and Energy*; UNESCO: Paris, France, 2014.
5. Siebert, S.; Burke, J.; Faures, J.M.; Frenken, K.; Hoogeveen, J.; Döll, P.; Portmann, F.T. Groundwater use for irrigation—A global inventory. *Hydrol. Earth Syst. Sci.* **2010**, *14*, 1863–1880. [CrossRef]
6. Gerten, D.; Heck, V.; Jägermeyr, J.; Bodirsky, B.L.; Fetzer, I.; Jalava, M.; Kummu, M.; Lucht, W.; Rockström, J.; Schaphoff, S.; et al. Feeding ten billion people is possible within four terrestrial planetary boundaries. *Nat. Sustain.* **2020**, *3*, 200–208. [CrossRef]
7. Boretti, A.; Rosa, L. Reassessing the projections of the World Water Development Report. *NPJ Clean Water* **2019**, *2*, 15. [CrossRef]
8. United Nations World Water Assessment Programme. *The United Nations World Water Development Report 2018*; United Nations Educational, Scientific and Cultural Organization: New York, NY, USA, 2018. Available online: www.unwater.org/publications/world-water-development-report-2018/ (accessed on 26 May 2022).
9. Sayl, K.N.; Muhammad, N.S.; El-Shafie, A. Robust approach for optimal positioning and ranking potential rainwater harvesting structure (RWH): A case study of Iraq. *Arab. J. Geosci.* **2017**, *10*, 413. [CrossRef]
10. Alwan, I.A.; Aziz, N.A.; Hamoodi, M.N. Potential water harvesting sites identification using spatial multi-criteria evaluation in Maysan Province, Iraq. *ISPRS Int. J. Geo-Inf.* **2020**, *9*, 235. [CrossRef]
11. World Economic Forum Annual Meeting. Shared Norms for the New Reality, Davos-Klosters, Switzerland, 26–30 January 2011. Available online: www.weforum.org (accessed on 26 May 2022).
12. Falkenmark, M.; Widstrand, C. Population and water resources: A delicate balance. *Popul. Bull.* **1992**, *47*, 1–36.
13. Wolf, A. Conflict and cooperation along international waterways. *Water Policy* **1998**, *1*, 251–265. [CrossRef]

14. U.S. Department of Agriculture (USDA). Foreign Agricultural Service. Middle East and Central Asia: Continued Drought in 2009/2010 Threatens Greater Food Grain Shortages. 2008. Available online: http://www.pecad.fas.usda.gov/highlights/2008/09/mideast_cenasia_drought/ (accessed on 16 September 2008).
15. Integrated Regional Information Networks. Syria: Drought Pushing Millions into Poverty. 2010. Available online: http://www.irinnews.org/Report/90442/SYRIA-Drought-pushing-millionsinto-poverty (accessed on 26 May 2022).
16. Michel, D.; Pandya, A.; Hasnain, S.I.; Sticklor, R.; Panuganti, S. *Water Challenges and Cooperative Response in the Middle East and North Africa*; Brookings Institution: Washington, DC, USA, 2012. Available online: http://www.brookings.edu/research/papers/2012/11/water-security-middle-east-iwf (accessed on 26 May 2022).
17. World Bank. *Making the Most of Scarcity: Accountability for Better Water Management Results in the Middle East and North Africa*; The MENA Development Report; The World Bank: Washington, DC, USA, 2007.
18. Kandeel, A. Climate Change: The Middle East Faces a Water Crisis. 2018. Available online: http://www.mei.edu/content/article/climate-change-middle-east-faces-water-crisis (accessed on 26 May 2022).
19. Procházka, P.; Hönig, V.; Maitah, M.; Pljučarská, I.; Kleindienst, J. Evaluation of water scarcity in selected countries of the Middle East. *Water* **2018**, *10*, 1482. [CrossRef]
20. de Vries, J.J.; Simmers, I. Groundwater recharge: An overview of process and challenges. *Hydrogeol. J.* **2002**, *10*, 5–17. [CrossRef]
21. Milewski, A.; Sultan, M.; Yan, E.; Becker, R.; Abdeldayem, A.; Soliman, F.; Gelil, K.A. A remote sensing solution for estimating runoff and recharge in arid environments. *J. Hydrol.* **2009**, *373*, 1–14. [CrossRef]
22. Mohamed, A.; Ahmed, E.; Alshehri, F.; Abdelrady, A. The groundwater flow behavior and the recharge in the Nubian Sandstone Aquifer System during the wet and arid periods. *Sustainability* **2022**, *14*, 6823. [CrossRef]
23. Mohamed, A.; Asmoay, A.; Alshehri, F.; Abdelrady, A.; Othman, A. Hydro-geochemical applications and multivariate analysis to assess the water–rock interaction in arid environments. *Appl. Sci.* **2022**, *12*, 6340. [CrossRef]
24. Tapley, B.D.; Bettadpur, S.; Watkins, M. The Gravity Recovery and Climate Experiment: Mission Overview and Early Results. *Geophys. Res. Lett.* **2004**, *31*, L09607. [CrossRef]
25. Syed, T.H.; Famiglietti, J.S.; Chen, J.; Rodell, M.; Seneviratne, S.I.; Viterbo, P.; Wilson, C.R. Total basin discharge for the Amazon and Mississippi River basins from GRACE and 20 a land-atmosphere water balance. *Geophys. Res. Lett.* **2005**, *32*, L24404. [CrossRef]
26. Crowley, J.W.; Mitrovica, J.X.; Bailey, R.C.; Tamisiea, M.E.; Davis, J.L. Annual variations in water storage and precipitation in the Amazon Basin: Bounding sink terms in the terrestrial hydrological balance using GRACE satellite gravity data. *J. Geod.* **2008**, *82*, 9–13. [CrossRef]
27. Xavier, L.; Becker, M.; Cazenave, A.; Longuevergne, L.; Llovel, W.; Filho, O.C.R. Interannual variability in water storage over 2003–2008 in the Amazon Basin from GRACE space gravimetry, in situ river level and precipitation data. *Remote Sens. Environ.* **2010**, *114*, 1629–1637. [CrossRef]
28. Papa, F.; Frappart, F.; Malbeteau, Y.; Shamsudduha, M.; Vuruputur, V.; Sekhar, M.; Ramillien, G.; Prigent, C.; Aires, F.; Pandey, R.K.; et al. Satellite-derived surface and sub-surface water storage in the Ganges–Brahmaputra River Basin. *J. Hydrol. Reg. Stud.* **2015**, *4*, 15–35. [CrossRef]
29. Rodell, M.; Famiglietti, J.S.; Chen, J.; Seneviratne, S.I.; Viterbo, P.; Holl, S.; Wilson, C.R. Basin scale estimates of evapotranspiration using grace and other observations. *Bull. Am. Meteorol. Soc.* **2004**, *31*, 10–13. [CrossRef]
30. Ahmed, M.; Sultan, M.; Wahr, J.; Yan, E. The use of GRACE data to monitor natural and anthropogenic induced variations in water availability across Africa. *Earth-Sci. Rev.* **2014**, *136*, 289–300. [CrossRef]
31. Śliwińska, J.; Wińska, M.; Nastula, J. Validation of GRACE and GRACE-FO mascon data for the study of polar motion excitation. *Remote Sens.* **2021**, *13*, 1152. [CrossRef]
32. Mohamed, A.; Sultan, M.; Ahmed, M.; Yan, E.; Ahmed, E. Aquifer recharge, depletion, and connectivity: Inferences from GRACE, land surface models, and geochemical and geophysical data. *Bull. Geol. Soc. Am.* **2017**, *129*, 534–546. [CrossRef]
33. Mohamed, A. Hydro-geophysical study of the groundwater storage variations over the Libyan area and its connection to the Dakhla basin in Egypt. *J. Afr. Earth Sci.* **2019**, *157*, 103508. [CrossRef]
34. Mohamed, A. Gravity based estimates of modern recharge of the Sudanese area. *J. Afr. Earth Sci.* **2020**, *163*, 103740. [CrossRef]
35. Mohamed, A. Gravity applications in estimating the mass variations in the Middle East: A case study from Iran. *Arab. J. Geosci.* **2020**, *13*, 364. [CrossRef]
36. Mohamed, A. Gravity applications to groundwater storage variations of the Nile Delta Aquifer. *J. Appl. Geophys.* **2020**, *182*, 104177. [CrossRef]
37. Mohamed, A.; Ragaa Eldeen, E.; Abdelmalik, K. Gravity based assessment of spatio-temporal mass variations of the groundwater resources in the Eastern Desert, Egypt. *Arab. J. Geosci.* **2021**, *14*, 500. [CrossRef]
38. Mohamed, A.; Gonçalvès, J. Hydro-geophysical monitoring of the North Western Sahara Aquifer System's groundwater resources using gravity data. *J. Afr. Earth Sci.* **2021**, *178*, 104188. [CrossRef]
39. Taha, A.I.; Al Deep, M.; Mohamed, A. Investigation of groundwater occurrence using gravity and electrical resistivity methods: A case study from Wadi Sar, Hijaz Mountains, Saudi Arabia. *Arab. J. Geosci.* **2021**, *14*, 334. [CrossRef]
40. Mohamed, A.; Abdelrahman, K.; Abdelrady, A. Application of time—Variable gravity to groundwater storage fluctuations in Saudi Arabia. *Front. Earth Sci.* **2022**, *10*, 873352. [CrossRef]

41. Mohamed, A.; Al Deep, M.; Othman, A.; Taha Al Alshehri, F.; Abdelrady, A. Integrated geophysical assessment of ground-water potential in southwestern Saudi Arabia. *Front. Earth Sci.* **2022**, *10*, 937402. [CrossRef]
42. Mohamed, A.; Faye, C.; Othman, A.; Abdelrady, A. Assessment of the global variability of terrestrial water storage in Senegal using gravity data. *Remote Sens.* 2022, *under review*.
43. Watkins, M.M.; Wiese, D.N.; Yuan, D.N.; Boening, C.; Landerer, F.W. Improved methods for observing Earth's time variable mass distribution with GRACE using spherical cap mascons. *J. Geophys. Res. Solid Earth* **2015**, *120*, 2648–2671. [CrossRef]
44. Milyukov, V.K.; Yeh, H.C. Next generation space gravimetry: Scientific tasks, concepts, and realization. *Astron. Rep.* **2018**, *62*, 1003–1012. [CrossRef]
45. Rodell, M.; Houser, P.R.; Jambor, U.; Gottschalck, J.; Mitchell, K.; Meng, C.-J.; Arsenault, K.; Cosgrove, B.; Radakovich, J.; Bosilovich, M.; et al. The global land data Assimilation system. *Bull. Am. Meteorol. Soc.* **2004**, *85*, 381–394. [CrossRef]
46. Rodell, M.; Chen, J.; Kato, H.; Famiglietti, J.S.; Nigro, J.; Wilson, C.R. Estimating groundwater storage changes in the Mississippi River basin (USA) using GRACE. *Hydrogeol. J.* **2009**, *15*, 159–166. [CrossRef]
47. Moiwo, J.; Tao, F.; Lu, W. Estimating soil moisture storage change using quasiterrestrial water balance method. *Fuel Energy Abstr.* **2011**, *107*, 25–34.
48. Ahmed, M.; Sultan, M.; Yan, E.; Wahr, J. Assessing and improving land surface model outputs over Africa using GRACE, feld, and remote sensing data. *Surv. Geophys.* **2016**, *37*, 529–556. [CrossRef]
49. Mohamed, A.; Al Deep, M. Depth to the bottom of the magnetic layer, crustal thickness, and heat flow in Africa: Inferences from gravity and magnetic data. *J. Afr. Earth Sci.* **2021**, *179*, 104204. [CrossRef]
50. Mohamed, A.; Abu El Ella, E.M. Magnetic applications to subsurface and groundwater investigations: A case study from Wadi El Assiuti, Egypt. *Int. J. Geosci.* **2021**, *12*, 77–101. [CrossRef]
51. Al Deep, M.; Araffa, S.A.S.; Mansour, S.A.; Taha, A.I.; Mohamed, A.; Othman, A. Geophysics and remote sensing applications for groundwater exploration in fractured basement: A case study from Abha Area, Saudi Arabia. *J. Afr. Earth Sci.* **2021**, *184*, 04368. [CrossRef]
52. Mohamed, A.; Al Deep, M.; Abdelrahman, K.; Abdelrady, A. Geometry of the magma chamber and curie point depth beneath Hawaii Island: Inferences from magnetic and gravity data. *Front. Earth Sci.* **2022**, *10*, 847984. [CrossRef]
53. Othman, A. Measuring and Monitoring Land Subsidence and Earth Fissures in Al-Qassim Region, Saudi Arabia: Inferences from InSAR. In *Advances in Remote Sensing and Geo Informatics Applications, Proceedings of the Conference of the Arabian Journal of Geosciences, CAJG 2018, Hammamet, Tunisia, 12–15 November 2018*; El-Askary, H., Lee, S., Heggy, E., Pradhan, B., Eds.; Advances in Science, Technology & Innovation (IEREK Interdisciplinary Series for Sustainable Development); Springer: Cham, Switzerland, 2019. [CrossRef]
54. Voss, K.A.; Famiglietti, J.S.; Lo, M.; De Linage, C.; Rodell, M.; Swenson, S. Groundwater depletion in the Middle East from GRACE with implications for transboundary water management in the Tigris–Euphrates–western Iran region. *Water Resour. Res.* **2013**, *49*, 904–914. [CrossRef] [PubMed]
55. Sissaskian, V.K.; Fouad, S.F.A. *Geological Map of Iraq, Scale 1:1,000,000*, 4th ed.; Iraq Geological Survey: Baghdad, Iraq, 2012.
56. Numan, M.S. A plate tectonic scenario for the phanerozoic succession in Iraq. *Iraqi Geol. J.* **1997**, *30*, 89–90.
57. Aqrawi, A. Paleozoic stratigraphy and petroleum systems of the Western and Southwestern Deserts of Iraq. *GeoArabia* **1998**, *3*, 229–248. [CrossRef]
58. Hessami, K.; Koyi, H.A.; Talbot, C.J. The significance of strike-slip faulting in the basement of the Zagros fold and thrust belt. *J. Pet. Geol.* **2001**, *24*, 5–28. [CrossRef]
59. Al-Jiburi, H.K.; Al-Basrawi, N.H. Hydrogeological map of Iraq, scale 1:1,000,000. *Iraqi Bull. Geol. Min.* **2015**, *11*, 17–26.
60. Krasny, J.; Alsam, S.; Jassim, S.Z. Hydrology. In *Geology of Iraq*; Jassim, S.Z., Goff, J.C., Eds.; Dolin, Prague and Moravian Museum: Prague, Czech Republic, 2006; pp. 251–287.
61. Saleh, S.A.; Al-Ansari, N.; Abdullah, T. Groundwater hydrology in Iraq. *J. Earth Sci. Geotech. Eng.* **2020**, *10*, 55–197.
62. Alsam, S.; Jassim, S.Z.; Hanna, F. *Water Balance of Iraq: Stage 2, Geological and Hydrogeological Conditions*; Report; Ministry of Irrigation: Baghdad, Iraq, 1990.
63. Domemico, P.A.; Schwartz, F.W. *Physical and Chemical Hydrogeology*; John Wiley and Sons, Inc.: New York, NY, USA, 1998; p. 506.
64. Araim, H. *Geological Map of Iraq 1:1,000,000 Series, Sheet 5, Hydrogeological Map of Iraq*; The Geological Survey of Iraq: Erbil, Iraq, 1991.
65. Luthcke, S.B.; Sabaka, T.J.; Loomis, B.D.; Arendt, A.A.; McCarthy, J.J.; Camp, J. Antarctica, Greenland, and Gulf of Alaska land-ice evolution from an iterated GRACE global mascon solution. *J. Glaciol.* **2013**, *59*, 216. [CrossRef]
66. Save, H.; Bettadpur, S.; Tapley, D.D. High resolution CSR GRACE RL05 mascons. *J. Geophys. Res. Solid Earth* **2016**, *121*, 7547–7569. [CrossRef]
67. Wiese, D.N.; Landerer, F.W.; Watkins, M.M. Quantifying and reducing leakage errors in the JPL RL05M GRACE mascon solution. *Water Resour. Res.* **2016**, *52*, 7490–7502. [CrossRef]
68. Save, H. CSR GRACE and GRACE-FO RL06 Mascon Solutions v02. 2020. Available online: http://www2.csr.utexas.edu/grace/RL06_mascons.html (accessed on 1 March 2022).
69. Tiwari, V.M.; Wahr, J.; Swenson, S. Dwindling groundwater resources in northern India, from satellite gravity observations. *Geophys. Res. Lett.* **2009**, *36*, L18401. [CrossRef]
70. Gonçalvès, J.; Petersen, J.; Deschamps, P.; Hamelin, B.; Baba-Sy, O. Quantifying the modern recharge of the "fossil" Sahara aquifers. *Geophys. Res. Lett.* **2013**, *40*, 2673–2678. [CrossRef]

71. Hassan, A.A.; Jin, S.G. Water cycle and climate signals in Africa observed by satellite gravimetry. In *IOP Conference Series: Earth and Environmental Science, Proceedings of the 35th International Symposium on Remote Sensing of Environment (ISRSE35), Beijing, China, 22–26 April 2013*; IOP Publishing: Bristol, UK, 2014; Volume 17, p. 012149. [CrossRef]
72. Sultan, M.; Sturchio, N.C.; Alsefry, S.; Emil, M.K.; Ahmed, M.; Abdelmohsen, K.; AbuAbdullah, M.M.; Yan, E.; Save, H.; Alharbi, T.; et al. Assessment of age, origin, and sustainability of fossil aquifers: A geochemical and remote sensing-based approach. *J. Hydrol.* **2019**, *576*, 325–341. [CrossRef]
73. Bhanja, S.N.; Zhang, X.; Wang, J. Estimating long-term groundwater storage and its controlling factors in Alberta, Canada. *Hydrol. Earth Syst. Sci.* **2018**, *22*, 6241–6255. [CrossRef]
74. Richey, A.S.; Thomas, B.F.; Lo, M.-H.; Reager, J.T.; Famiglietti, J.S.; Voss, K.; Swenson, S.; Rodell, M. Quantifying renewable groundwater stress with GRACE. *Water Resour. Res.* **2015**, *51*, 5217–5238. [CrossRef]
75. Trigo, R.M.; Gouveia, C.M.; Barriopedro, D. The intense 2007–2009 drought in the Fertile Crescent: Impact and associated atmospheric circulation. *Agric. For. Meteorol.* **2010**, *150*, 1245–1257. [CrossRef]
76. Tourian, M.J.; Elmi, O.; Chen, Q.; Devaraju, B.; Roohi, S.; Sneeuw, N. A spaceborne multisensor approach to monitor the desiccation of Lake Urmia in Iran. *Remote Sens. Environ.* **2015**, *156*, 349–360. [CrossRef]
77. Divins, D. *Total Sediment Thickness of the World's Oceans and Marginal Seas*; NOAA National Geophysical Data Center: Boulder, CO, USA, 2003.